Research Article

Junjun Shen, Kongquan Chen*, Yang Liu, Fangfang Chen, Xiaosong Qiu, Xiaoqiang Ma, and Jianghui Meng

Sedimentary facies of Paleogene lacustrine dolomicrite and implications for petroleum reservoirs in the southern Qianjiang Depression, China

https://doi.org/10.1515/geo-2019-0042
Received Dec 01, 2018; accepted Jul 26, 2019

Abstract: Paleogene lacustrine dolomicrite of Unit II of the lower Xingouzui Formation in the southern part of the Qianjiang Depression, China forms "tight carbonate" hydrocarbon reservoirs that can be divided into the following four dolomicrite types: dolomicrite, muddy dolomicrite, sandy dolomicrite, and gypsiferous dolomicrite. These four dolomicrite types occur in the following three distinct combinations, which are referred to as subfacies: (1) interbedded dolomicrite (or sandy dolomicrite) and dark-gray siliciclastic mudstone, interpreted as open lacustrine deposits, (2) grayish-dark siliciclastic mudstone with thinly-bedded muddy dolomicrite or gypsiferous dolomicrite, interpreted as restricted lacustrine deposits, and (3) grayish-green mudstone with thinly-bedded brown-yellow siltstone, interpreted as lacustrine shoreline deposits. The spatial distribution of these subfacies was controlled by the paleo-provenance system, paleo-microgeomorphology, and lake level fluctuations. In the open lacustrine subfacies, dolomicrite or sandy dolomicrite are often vertically interbedded with dark argillite rocks, forming a suitable petroleum source rock-reservoir association. The dolomicrite and sandy dolomicrite reservoirs possess many secondary crystalline pores and few dissolution pores, with mesopore porosities in the range of 15%–25%. The dark mud shale interval has total organic carbon (TOC) values exceeding 4% (averaging 1.29%). The organic matter is mainly type II_2, with vitrinite reflectance values averaging 0.57, which indicates potential for the generation of immature oil. The oil-source correlation results indicated that the n-alkanes of the crude oil and source rock samples from Unit II of the lower Xingouzui Formation exhibit single peak values, with a main peak (post-peak) in C_{22} and a Pr/Ph ratio < 1 in a $C_{29}20R > C_{27}20R > C_{28}20R$ distribution. These features indicate that source-reservoir interbedding is characteristic of self-sourced reservoirs. The interbedded dolomicrite (or sandy dolomicrite) and dark-gray siliciclastic mudstone, *i.e.*, subfacies (1), is a favorable target for hydrocarbons in the study area.

Keywords: Qianjiang Depression; Dolomite reservoir; Sedimentary facies; Self-sourced reservoir; Favorable depositional facies

***Corresponding Author: Kongquan Chen:** Hubei Cooperative Innovation Center of Unconventional Oil and Gas of Yangtze University, Wuhan, Hubei 430100, China; Email: 705194434@qq.com
Junjun Shen: Key Laboratory of Exploration Technologies for Oil and Gas Resources (Yangtze University), Ministry of Education, Wuhan, Hubei 430100, China; Hubei Cooperative Innovation Center of Unconventional Oil and Gas of Yangtze University, Wuhan, Hubei 430100, China
Yang Liu: Explorating Department of China National Offshore Oil Corporation, Beijing 100010, China
Fangfang Chen: Research Institute of Exploration and Development, Tarim Oilfield Company, PetroChina, Korla,Xinjiang 841000, China
Xiaosong Qiu: Langfang Branch of PetroChina Research Institute of Petroleum Exploration and Development, Langfang, Hebei 065000, China
Xiaoqiang Ma: Research Institute of China National Offshore Oil Corporation, Beijing, 100027, China
Jianghui Meng: Hubei Cooperative Innovation Center of Unconventional Oil and Gas of Yangtze University, Wuhan, Hubei 430100, China

1 Introduction

In China, restricted lacustrine carbonate deposits are present in Permian, Cretaceous, lower Paleogene, and upper Neogene strata [1]. Much of this lacustrine carbonate consists of dolomite and is widespread throughout China. For example, lacustrine dolomite is found throughout the Permian units in the Santanghu Basin, the Paleogene units

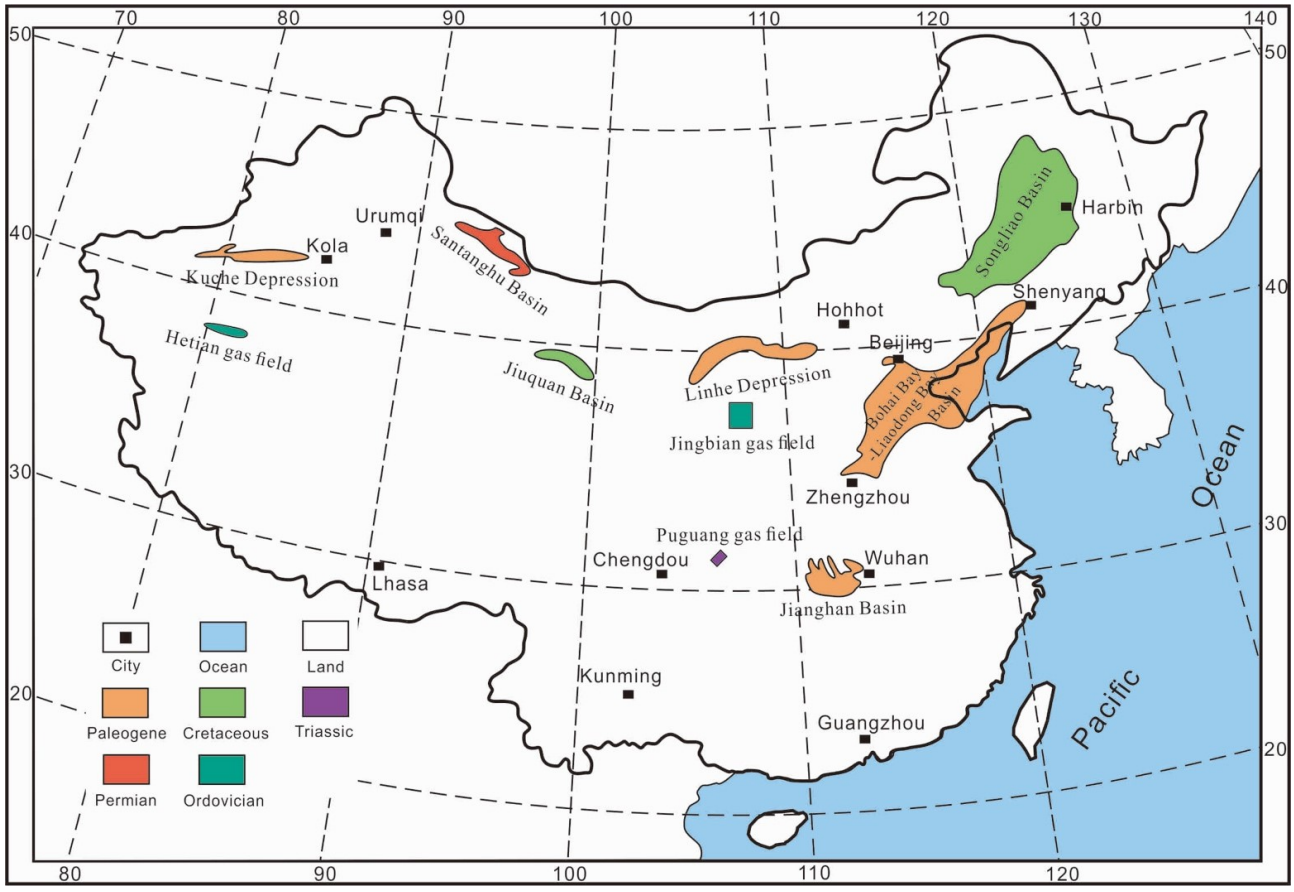

Figure 1: Spatial and temporal distributions of basins with lacustrine dolomite and gas fields with marine dolomite reservoirs in China

in the Kuche Depression, the Lower Cretaceous units in the Jiuquan Basin, the Cretaceous-Paleogene units in the Linhe Depression of Inner Mongolia, the Paleogene units in the Jianghan Basin, the Late Cretaceous units in the Songliao Basin, and the Paleogene units in the Bohai Bay-Liaodong Bay Basin (Figure 1). Previous studies of these strata have proposed specific sedimentary models regarding the factors controlling lacustrine carbonate deposition [2–6]. For example, in both eastern offshore fault-bounded basins and central inland basins, the deposition of lacustrine carbonates was controlled primarily by lake level fluctuations, lake basin paleogeomorphology, and the sediment paleo-provenance system. Most of these previous studies, however, have focused on the eastern offshore fault-bounded basins, whereas few have evaluated the lacustrine carbonates in the central inland basins. Furthermore, few studies have focused on either the paleoclimate controls or the properties of the lacustrine water during deposition [7–9].

Many of the extensive oil and gas fields in China are located in marine carbonate strata that are composed primarily of dolomite, including Ordovician reservoirs in the Hetian gas field in the Tarim Basin in Xinjiang, Ordovician reservoirs in the Jingbian gas field in the Erdos Basin in Inner Mongolia, and Triassic reservoirs in the Puguang gas field in the Sichuan Basin (Figure 1). Several previous studies have indicated that these carbonate strata accumulated initially as limestone, after which they were subsequently altered to dolomite. These studies also found that the main controls on reservoir formation include the dominant facies belt, the primary rock (limestone) fabric, dolomitization, and faulting during deep burial [10–14]. These studies, however, primarily focused on deeply-buried Paleozoic marine carbonate strata, whereas shallow-buried Mesozoic or Cenozoic lacustrine carbonate strata have received little attention.

Previous investigations of reservoirs in Mesozoic or Cenozoic carbonate strata in China have been largely macroscopic in scale and have focused on the factors controlling regional tectonics, fault systems, and sedimentary environments rather than the development of the dolomite reservoirs [2, 15, 16]. Many studies interpret extensive dolomites in the geologic record to be of secondary replacement origin, and their genetic models mainly in-

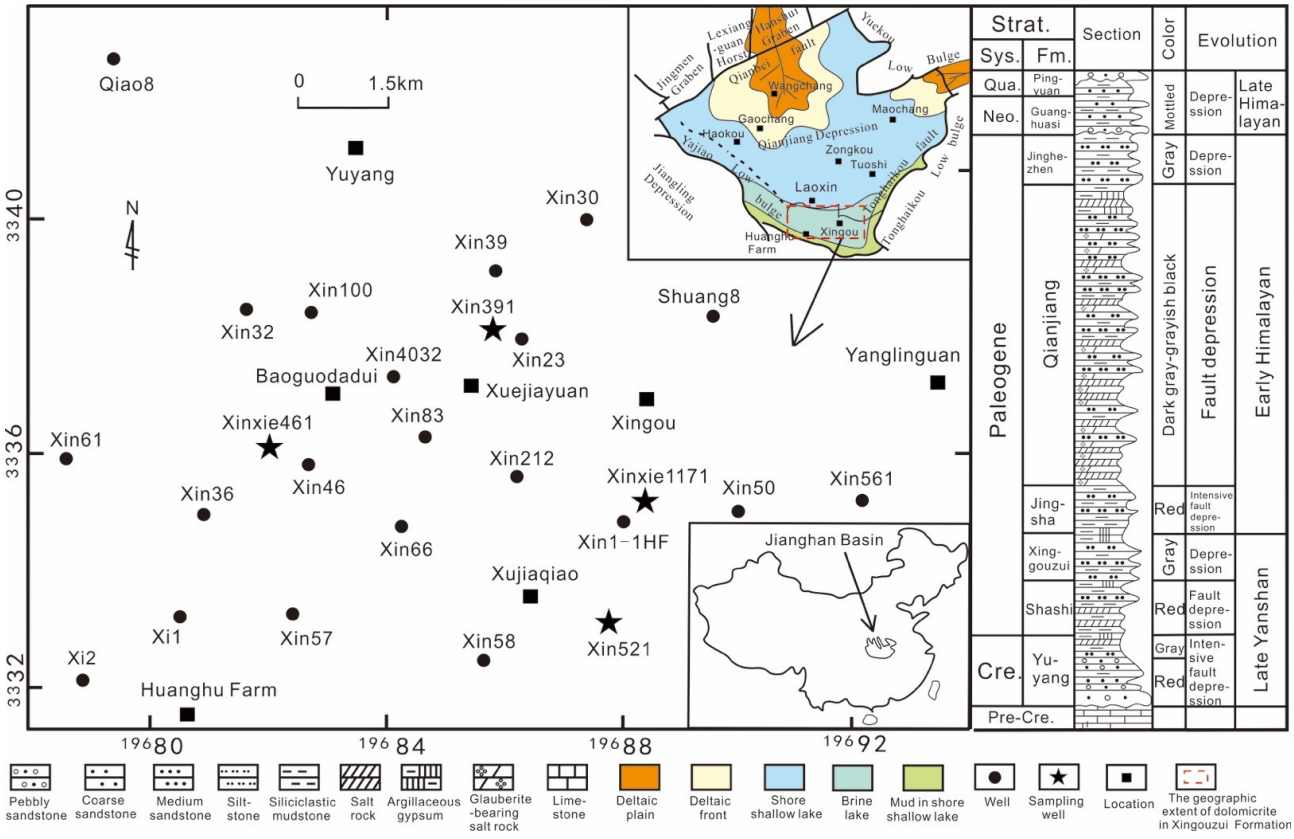

Figure 2: Well locations and Paleogene depositional environments of the Qianjiang Depression
The stratigraphic column of the Qianjiang Depression is shown on the right.
Note: The stratigraphic column is a composite column derived from numerous wells in the Qianjiang Depression.

clude seepage-reflux and burial mode [14, 17]. Few researchers have attempted to investigate carbonate reservoirs in China from a microscale perspective (*i.e.*, the impacts of rock structure, dolomitization, and diagenesis on the reservoirs). This study addresses some of these unresolved issues by presenting a study of dolomicrite in the Paleogene Xingouzui Formation in the southern Qianjiang Depression (Figure 2). In this setting, the rock structure is relatively simple and is dominated by dolomicrite or microcrystalline dolomite [17].

2 Geologic setting

The Qianjiang Depression is located in the center of the Jianghan Basin (Figure 2). The Qianjiang Depression covers an area of approximately 2,500 km^2 and is bound by two approximately northeast-trending margin faults [18]. The Qianjiang Depression is bounded on the northwest by the northeast-trending Qianbei Fault Zone and the associated Jingmen graben, Lexiangguan horst, Hanshui graben, and Yonglonghe uplift (Figure 2). The Qianjiang Depression is bounded on the southeast by the northeast-trending Tonghaikong Fault and the associated Tonghaikou uplift (Figure 2). The Qianjiang Depression is bounded on the northeast by the Yuekou uplift and is bounded on the southwest by the Yajiao uplift and Xingou uplift (Figure 2).

Drilling has revealed that the strata of the Qianjiang Depression, from top to bottom, consist of the Quaternary Pingyuan Formation; the Neogene Guanghuasi Formation; the Paleogene Jinghezhen, Qianjiang, Jingsha, Xingouzui, and Shashi Formations; and the Cretaceous Yuyang Formation (Figure 2). The Pingyuan Formation unconformably overlies the Guanghuasi Formation, and the Guanghuasi unconformably overlies the Jinghezhen Formation. The other formation contacts are conformable.

The Qianjiang Depression is interpreted as having been formed during three tectonic evolutionary phases [19], which are listed adjacent to the stratigraphic column in Figure 2. The oldest tectonic phase is the Late Yanshan extensional fault depression phase, which is thought to have been coincident with the accumulation of

the Cretaceous Yuyang Formation through the Paleocene Xingouzui Formation. The middle tectonic phase is the Early Himalayan strike-slip extensional phase, which is thought to have been coincident with the accumulation of the Paleogene Jingsha Formation through the Paleogene Jinghezhen Formation. The youngest tectonic phase is the Late Himalayan compression, uplift, and erosion phase, which is believed to have begun during the accumulation of the Neogene Guanghuasi Formation and is still occurring today (Figure 2).

The Paleogene Xingouzui Formation, which is the subject of this study, is 400–600 m thick in the Qianjiang Depression and consists of siliciclastic mudstone, siltstone, argillaceous dolomite, and dolomite. The Xingouzui Formation is divided, from top to bottom, into the following 5 units: (1) the upper Xingouzui Formation (UX), which is 200–300 m thick and consists predominantly of brown-red siliciclastic mudstone; (2) Unit I of the lower Xingouzui Formation (LXF), which is 100–120 m thick and consists predominantly of brown-red siliciclastic mudstone with gypsiferous mudstone; (3) Unit II of the LXF, which is 90–120 m thick and consists predominantly of interbedded dolomicrite and dark argillite; (4) a mud barrier unit, which is 20–30 m thick and consists predominantly of grayish siliciclastic mudstone; and (5) Unit III of the lower Xingouzui Formation, which is 100–150 m thick and consists predominantly of brown-red siliciclastic mudstone with siltstone.

Unit II of the LXF, which is a reservoir target, is divided into the following five subunits, from top to bottom (Figure 4): (1) the lower II 1+2 subunit, which is 20–30 m thick and consists predominantly of interbedded dolomicrite and dark argillite; (2) an upper mudstone subunit, which is 10–15 m thick and consists predominantly of grayish siliciclastic mudstone; (3) the lower II 3+4 subunit, which is 25–35 m thick and consists predominantly of grayish-yellow dolomicrite or sandy dolomicrite with siliciclastic mudstone or argillaceous gypsum; (4) a lower mudstone subunit, which is 15–20 m thick and consists predominantly of grayish siliciclastic mudstone; and (5) the lower II 5 subunit, which is 25–30 m thick and consists predominantly of grayish-yellow dolomicrite or muddy dolomicrite with siliciclastic mudstone or gypsiferous mudstone. Previous studies of Unit II of the Paleogene LXF in the southern Qianjiang Depression have indicated that these strata are impermeable and are non-commercial with respect to oil and gas production [19]. The reviews of wells Xin 23 and Xin 30 in the south (Figure 2) indicate that the dolomicrite beds of Unit II of the LXF are rich in oil and gas. Subsequent drilling, however, has achieved stable commercial oil flows from the dolomicrite by fracturing the entire Unit II of the LXF. For example, well Xinxie 1171 (Figure 2) produced oil at a rate of 12.5 bbl/d (barrels of oil per day) during stable production, whereas well Xinxie 461 (Figure 2) produced 11.35 bbl/d and well Xin 1-1HF (Figure 2) produced 48.5 bbl/d.

3 Sampling and analytical methods

For this study, a total of 336 samples were obtained from the full-hole coring of 4 wells (Xin 391, Xinxie 1171, Xinxie 461, and Xin 521) in Unit II of the Paleogene LXF in the Xingou Region (Figure 2). A total of 185 of the samples were from well Xin 391 (30 dolomite and 155 siliciclastic mudstone), 43 of the samples were from well Xinxie 1171 (6 dolomite and 37 siliciclastic mudstone), 38 of the samples were from well Xinxie 461 (2 dolomite and 36 siliciclastic mudstone), and 70 of the samples were from well Xin 521 (25 dolomite and 45 siliciclastic mudstone). Three crude oil samples were collected from Unit II of the LXF in wells Xinxie 461, Xin 391, and Xinxie 1171 (Figure 2). Conventional thin sections of all samples were examined using a polarized light microscope to ensure reliable classification and analysis. The samples were ground using agate mortars, sieved through a 200-mesh screen, and sealed in plastic sample bags in preparation for scanning electron microscopy (SEM), cathode luminescence, X-ray diffraction, total organic carbon (TOC) determination, rock-eval pyrolysis, kerogen SEM identification, vitrinite reflectance, two types of saturated hydrocarbon chromatography, and gas chromatography-mass spectrometry. Each sample weighed more than 10 g.

The reservoir samples were analyzed at the Geological Laboratory of Exploration and Development Institute of the Southwest Oil and Gas Company, SINOPEC (Beijing, China). A JSM-5500 field emission environmental scanning electron microscope was utilized for SEM observations, a CL8200-MK5 cathode luminescence microscope for cathode luminescence observations at room temperature, a Pore Master 33 mercury injection apparatus for mercury injection with a measurable pore diameter range of 6.4 nm to 950 μm, and a Philips X'pert-MPD X-ray diffractometer for X-ray diffraction analysis, which was designed to predict mineral types and contents based on its 2θ angle (a scanning range of 20°–40°) and spectrum strength.

Geochemical sample analyses were performed at the Geochemical Laboratory of the Global Environment and Water Resources Institute, Yangtze University (Jingzhou, China). A CS-344 Carbon/Sulfur Analyzer was used for the measurement of TOC values, a Leica AF6000 transmission-

reflection fluorescence microscope for microscopic measurements of kerogen compositions, a Leica MSP200 microphotometer for measurement of vitrinite reflectance, an OGE-II hydrocarbon evaluation station for measurement of the rock pyrolysis parameters, an Agilent (Agilent Technologies, Santa Clara, CA, USA) 7890A gas chromatograph for saturated hydrocarbon chromatography analysis, an Agilent 6890N gas chromatograph for saturated hydrocarbon chromatograms, and an Agilent 5973N mass selector for gas chromatography-mass spectrometry analysis.

For descriptions of carbonate rock hand specimens, the [20] carbonate classification terms were used. The carbonate rocks in the southern Qianjiang Depression were also classified in terms of their detrital, calcite, and dolomite contents [19, 21], whereas the crystal size was considered for the clean and pure dolomites [21].

4 Descriptions of the dolomicrite

Dolomite in Unit II of the LXF is only present in the southern Qianjiang Depression (Figure 2). In this area, the following four dolomite lithologies can be identified in Unit II: dolomicrite, muddy dolomicrite, sandy dolomicrite, and gypsiferous dolomicrite.

(1) ***Dolomicrite*** is grayish-yellow. It is the dominant rock type in the study area and is almost completely dolomitized. It contains few or no particles, has a homogeneous structure, and is dominated by beds without obvious sedimentary structures (Figures 3a, b, and c). The dolomite crystals are generally 3–5 μm in size and are xenotopic, with rough surfaces and non-embedded contacts. The contact boundaries are irregularly toothed (Figure 3c). The grain sizes range from 5–10 μm in size (Figure 3c), and thus the structures are not visible using a plane-polarized light microscope or a cathode luminescence microscope (Figures 3d and f). It is therefore impossible to infer the primary sedimentary structures of the limestone.

(2) ***Muddy dolomicrite*** is common in individual intervals of Unit II of the LXF and is characterized by thin interbedding or non-isopachous interbedding of grayish-yellow dolomicrite and dark argillite (Figures 3e and f). The dolomite beds are generally 0.5–20 mm thick, with a few reaching 50 mm. The thickness distribution of the siliciclastic mudstone is similar to that of the dolomites, but the former is usually thinner. The muddy dolomicrite is dominated by rhythmic deformed beds (Figure 3e) and is tight. Generally, the muddy dolomicrite is faulted along lithologic boundaries. The intercrystalline spaces of the dolomite are filled with masses of silky illite, such that the pore spaces are blocked (Figure 3g).

(3) ***Sandy dolomicrite*** is grayish-brown or grayish-yellow and moderately thick to thick-bedded (0.5–1 m thick). Bedding structures are not obvious in the core interiors, and most beds do not display obvious sedimentary structures (Figures 3h and i). The dolomicrite is poorly bedded (Figures 3j and k). In the sandy dolomicrite, sandy debris is dominant, with debris consisting of silty quartz and feldspar particles that are moderately sorted and rounded. In cathodoluminescence (CL) images, the dolomicrite has an orange color, the quartz particles are not luminescent, and the feldspar is primarily bright blue, but a few particles are green (Figure 3j). The quartz and feldspar particles are generally scattered throughout the dolomicrite as single particles.

(4) ***Gypsiferous dolomicrite:*** Gypsiferous rocks are common in the study area and are present as millimeter- to centimeter-sized hard gypsum columnar crystals and small nodules with a variety of occurrences, contents, and sizes. Gypsum often occurs in the following two such forms: (1) abundant small nodules of gypsum that do not exceed 5 mm in diameter (Figure 3l), which are mostly developed in well-bedded units within dolomicrite without obvious sedimentary structures. Gypsum in such occurrences often grades into, or is interbedded with, dolomicrite containing few or no gypsum nodules; (2) a few large nodules of gypsum that do not exceed 1 cm in diameter, which are distributed within beds of dolomicrite or interbedded dark argillite. The plot of gypsum nodule diameter vs. nodule number has a negative slope. The number of nodules is limited by the large nodule diameters (Figure 3m).

The 4 dolomicrite types described above (dolomicrite, muddy dolomicrite, sandy dolomicrite, and gypsiferous dolomicrite) occur in the following three distinct combinations, which are referred to as subfacies. Subfacies (1) is composed of interbedded dolomicrite or sandy dolomicrite and dark-gray siliciclastic mudstone. The dolomicrite and sandy dolomicrite are predominant, with a single bed thickness of approximately 1 m (Figure 4), although the bedding in the sandy dolomicrite is poorly defined (Figures 3j and k). In the transition belts of both lithologies, wave bedding, bioturbation, and variously deformed structures are common (Figures 3n, o, and p). Subfacies (2) is composed of grayish-dark siliciclastic mud-

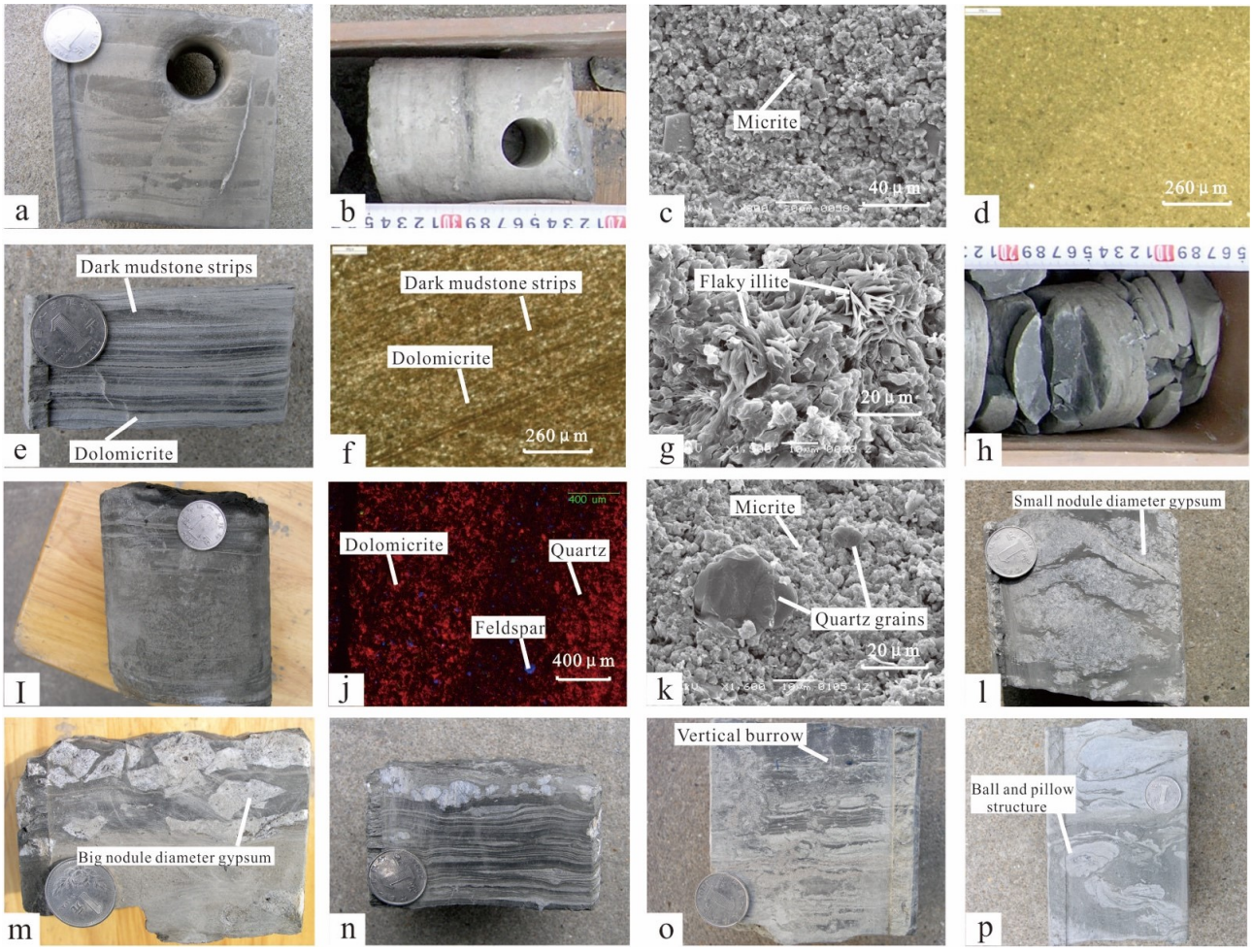

Figure 3: Textural, structural, and coring characteristics of the various dolomites in the study area
a: pure dolomicrite, X391, 1395.5 m, II 1+2; b: pure dolomicrite, XX461, 1295.5 m, II 1+2; c: dolomicrite, with rough crystal surface, xenotopic, in intercrystal non-plate contact, XX461, 1295.5 m, II 1+2, SEM; d: pure dolomicrite, XX1171, 820.2 m, II 3+4, plane-polarized light (-); e: unisopachous interbedding of dolomicrite and dark mudstone strips, X391, 1410 m, II 3+4; f: lamellar co-occurrence of dolomicrite and dark mudstone strips, XX1171, 814.7 m, II 3+4; g: silky, flaky illite attached to a dolomite aggregation surface, with blocked pores, XX1171, 860.2 m, II 5, SEM; h: sandy dolomicrite, XX461, 1290.94 m, II 1+2; i: sandy dolomicrite, X521, 971.11 m, II 1+2; j: sandy dolomicrite, with moderate sorting and rounded quartz and feldspar grains, poorly bedded, X521, 971.11 m, II 1+2; k: quartz grains embedded in a dolomite aggregate, poor sorting, X521, 1055.3 m, II 5, SEM; l: gypsiferous dolomicrite, most of a small-diameter gypsum nodule developed in dolomicrite, well bedded, X391, 1418.4 m, II 3+4; m: gypsiferous dolomicrite, part of a large-diameter gypsum nodule developed in dolomicrite, poorly sorted, X391, 1464 m, II 5; n: wave bedding in an open lacustrine sedimentary environment, X391, 1409 m, II 1+2; o: bioturbation structure, primary strata destroyed by intense bioturbation, in an open lacustrine sedimentary environment, X391, 1435 m, II 3+4; p: deformation structure, with ball and pillow structure in the interior, X391, 1476 m, II 5, in an open lacustrine sedimentary environment

stone with thinly-bedded muddy dolomicrite or gypsiferous dolomicrite (Figures 3l and m). The evaporite minerals within the argillite are extremely well developed (Figure 4) and are characterized by alternating vertical zones of small-diameter gypsum nodules and poorly bedded, large-diameter gypsum nodules. Subfacies (3) is composed of grayish-green mudstone with thinly-bedded muddy brown-yellow siltstone (Figure 4). In the study area, this subfacies is rare and is only found on the periphery of well Qiao 8, which is on the northeast margin of the study area (Figure 5).

5 Interpretations of the dolomicrite

5.1 Sedimentary characteristics

Unit II of the LXF in the Xingou Region is interpreted as having accumulated in a shallow lacustrine environ-

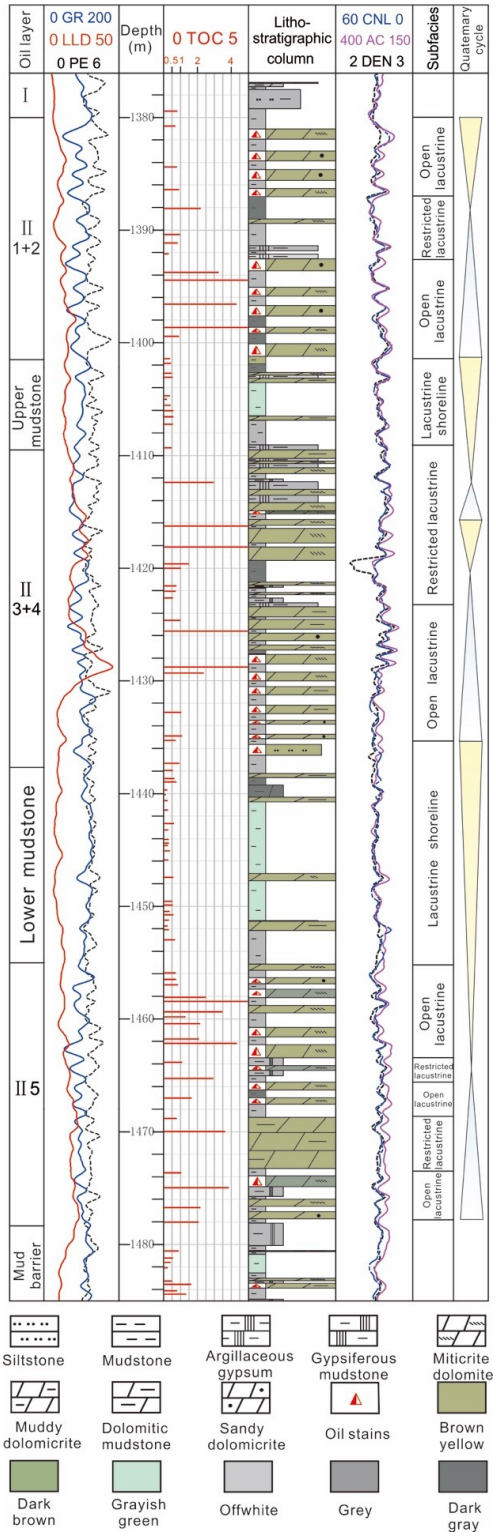

Figure 4: Generalized stratigraphic column of well Xin 391
GR = gamma-ray log; LLD = deep lateral log; PE = photoelectric cross-section log; CNL = neutron log; AC = acoustic log; DEN = density log; and TOC = total organic carbon

ment, as a result of the following factors: (1) rare terrigenous clastic particles in the study area, with extremely fine grain sizes (10–50 μm), which are scattered in mudstone or micritic dolomite, indicative of a relatively weak sedimentary hydrodynamic force as a result of being far from the shore; (2) the sedimentary structures predominantly consist of variously deformed structures, bioturbation structure, wave bedding, climbing ripple bedding, and wave-ripple bedding, indicative of a relatively shallow sedimentary water volume, which is greatly affected by lake waves; and (3) no oxidation color and sedimentary structure markers in a drought-exposed environment, with indistinct shore lacustrine deposition characteristics [17, 19]. As described below, the lacustrine sediments can be divided into the following depositional subfacies: open lacustrine, restricted lacustrine, and lacustrine shoreline.

(1) ***Open lacustrine subfacies:*** Subfacies (1), which is composed of interbedded dolomicrite (or sandy dolomicrite) and dark gray siliciclastic mudstone, is interpreted as open lacustrine deposits. In this subfacies, the frequent interbedding of dolomicrite or sandy dolomicrite and dark argillite rocks is indicative of rapid and frequent alterations of the sedimentary environment.

In the study area, the open lacustrine subfacies (1) tends to be enlarged in the region from Unit II 5 to Unit II 1+2 deposition. During the Unit II 5 deposition, the lake basin had reached its peak development and the water extended to a great depth, wherein the open lacustrine subfacies was deposited in a limited area within the Xinxie 461 – Xin 100 – Xin 392 – Xin 87 – Xin 87 – Xin 42 – Xin 132 – Xin 57 – Xin 89 well line (Figure 5b). When Unit II 3+4 was deposited, the lake basin shrank and the water became shallow, and the open lacustrine subfacies was extensively distributed to the north of the Xin 61 – Xin 32 – Xin 30 – Shuang 8 well line and south of the Xin 57 – Xin 46 – Xin 93 – Xin 83 – Xin 132 – Xin 561 well line (Figure 5c). During Unit II 1+2 deposition, the lake basin was at its lowest water level and the open lacustrine subfacies was distributed in the widest area. Thus, the open lacustrine subfacies represents the main sedimentary environment of the entire study area (Figure 5d). This subfacies is one that accumulated in topographically high areas of the shallow lake that were far from the sediment provenance region. The open lacustrine subfacies accumulated in a belt between the lowest water levels during dry periods and the normal wave baseline with relatively weak hydrodynamic energy, which was insufficient

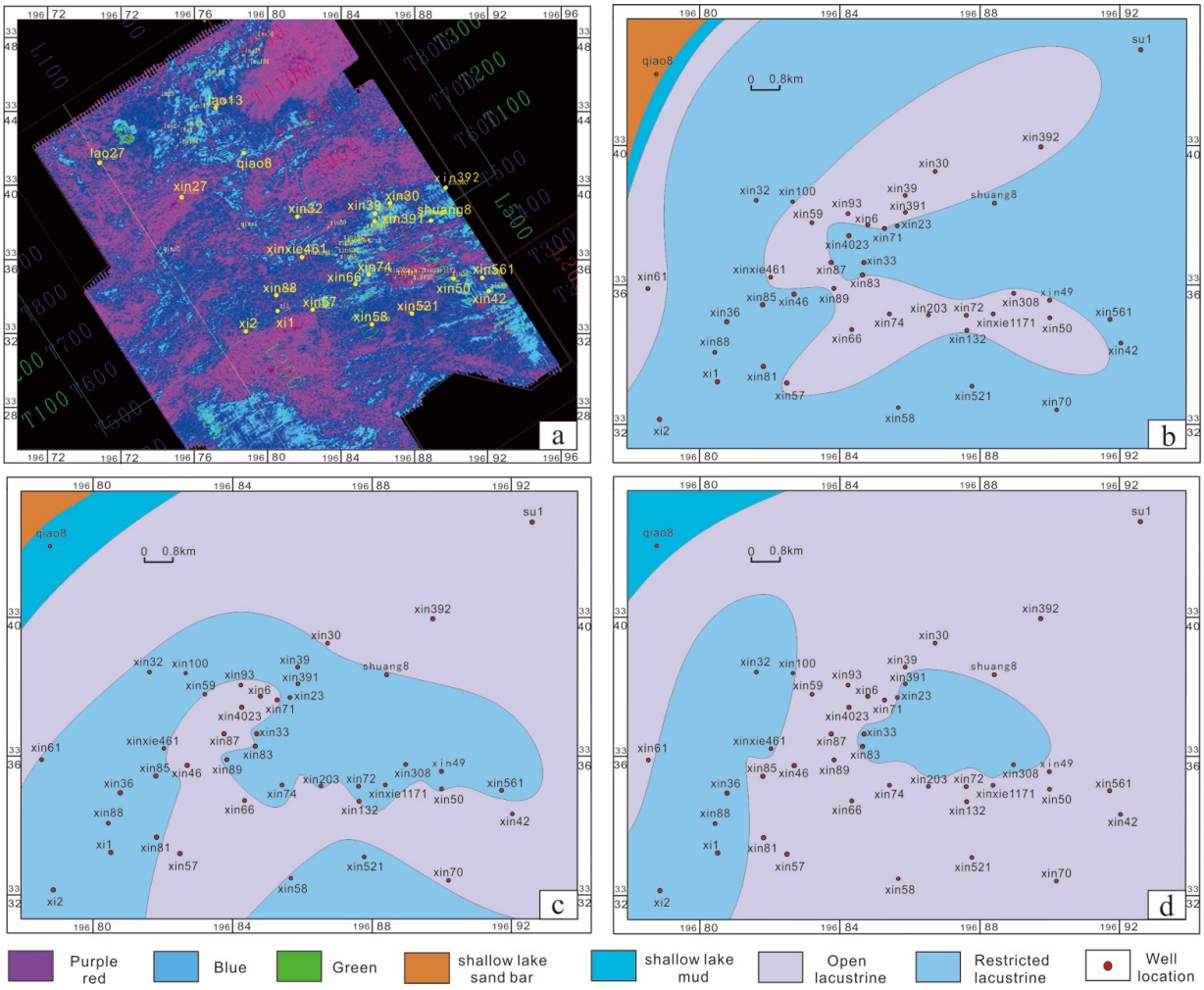

Figure 5: RMS attributes and lateral distributions of the sedimentary facies of Unit II of the LXF in the Xingou Region
a: RMS attributes from 80 ms below the top interface of Unit I to Unit II of the LXF; b: lateral distribution of the sedimentary facies of Unit II 5 of the LXF; c: lateral distribution of the sedimentary facies of Unit II 3+4 of the LXF; d: lateral distribution of the sedimentary facies of Unit II 1+2 of the LXF; RMS = root mean square amplitude

to form extensive granular or bioclastic carbonate rocks. When the lake level dropped, evaporation increased, resulting in increased salinity.

(2) ***Restricted lacustrine subfacies:*** Subfacies (2), which is composed of grayish-dark siliciclastic mudstone with thinly-bedded muddy dolomicrite or gypsiferous dolomicrite, is interpreted as restricted lacustrine deposits. This subfacies is one that accumulated in topographically low lake bottom areas between the open lacustrine and below the wave baseline, indicative of a restricted sedimentary environment.

In the study area, the restricted lacustrine subfacies tended to decrease in area from Unit II 5 to Unit II 1+2 deposition. During the Unit II 5 deposition, the restricted lacustrine subfacies was distributed in the widest area from the Xinxie 461 – Xin 100 – Xin 392 – Xin 87 – Xin 49 – Xin 42 – Xin 132 – Xin 57 – Xin 89 well line (Figure 5b). When Unit II 3+4 was deposited, the restricted lacustrine subfacies shrank to within the Xin 61 – Xin 30 – Xin 42 – Xin 74 – Xin 6 – Xin 46 – Xin 57 well line and within the Xin 58 – Xin 521 – Xin 70 well line (Figure 5c). During the Unit II 1+2 deposition, the restricted lacustrine subfacies further shrank to within the Xin 61 – Xin 100 – Xin 85 – Xin 81 well line and the Xin 83 – Xin 391 – Xin 49 – Xin 203 well line (Figure 5d).

(3) ***Lacustrine shoreline subfacies:*** Subfacies (3), which is composed of grayish-green mudstone with thinly-bedded brown-yellow siltstone, is interpreted as lacustrine shoreline deposits. The grayish-green mudstone is interpreted specifically as deposits of

shallow lacustrine mud, whereas the brown-yellow siltstone is interpreted as deposits of shallow lacustrine sandbars (Figure 4).

5.2 Development of the dolomicrite reservoirs

Comprehensive analysis of the 4 full-hole wells that were cored (including a total of 436.7 m of long core observations, SEM observations, cathode luminescence observations, and mercury injection of samples 36, 13, and 29) was used to determine the main accommodation types for the dolomite reservoirs based on the various types of microfacies found in the study area and their petrophysical properties. Based on this, the main factors controlling the shallow-buried lacustrine dolomite reservoirs in the study area were determined using a composite analysis of the genesis and diagenesis of the units.

5.2.1 Spatial descriptions of the dolomite reservoirs

From the detailed SEM observations and statistical analyses that were conducted by [15], the pores in the dolomite reservoirs associated with the various types of microfacies were found to be critical for hydrocarbon accommodation. The fractures of the reservoir were well developed and completely filled with gypsum.

(1) ***Pore characteristics:*** The pores in the dolomite reservoirs of Unit II of the LXF in the Xingou Region were inherited from the primary pores, which in turn were composed of dominant secondary intercrystalline pores and a few primary microbial pores, secondary intercrystalline dissolution pores, and mold pores.

Primary microbial pores consist of algae-microbe cavity pores with pore diameters of approximately 20 μm. Due to the low influence of mechanical compaction and recrystallization, the microbial cavity pores are generally well preserved and remain unfilled, and thus improve connectivity locally (Figure 6a). However, the pores are developed at a limited scale and are sparsely distributed, providing a smaller contribution to the reservoirs.

Intercrystalline pores are developed among the xenomorphic dolomicrite crystals, indicative of selective fabric pores. These types of rocks are supported by crystal grains, and their intercrystalline spaces are not filled with cement. Thus, they provide good accommodation in an irregular polyhedron shape, with pore diameters of approximately 2–4 μm (Figure 6b). They are one of the main contributors to the reservoirs in the study area.

Intercrystalline dissolution pores in the dolomite are occupied by acidic fluids that enter the pores later, during diagenesis. These acidic fluids partially dissolve the dolomite crystals and enlarge the intercrystalline pores. Finally, the shape of the intercrystalline pores is irregular, and their diameters are generally 2–10 μm, which is larger than those of the dolomite crystals (Figure 6c). As dissolution increases, the intercrystalline pores become extremely large dissolution pores that are internally filled with micritic dolomite or secondary albite, which forms due to burial (Figure 6d). These types of pores are less developed in the study area and are poorly connected, thus contributing less to the reservoirs.

Mold pores are fabric-selective and form because of the selective dissolution of bioclastic deposits during early mineral stabilization (Figure 6e). Both the extensive small gypsum nodules and the large gypsum nodules in the dolomite remain undissolved and are well preserved, which indicates that the dolomite reservoirs in the study area were formed during early diagenesis. These types of pores are undeveloped and contribute less to the reservoirs.

(2) ***Fracture characteristics:*** Based on bulk core and SEM observations, the fractures in the Xingou Region can be divided into structural and dissolution fractures.

Structural fractures are well developed in the study area, but are generally flat, high-angle fractures and are not oblique to each other (Figure 6f), indicating that they were not formed during multiple phases. Lithological observations and statistics indicate that the fractures were later filled with gypsum. Cathodoluminescence analysis indicates that the fractures were subjected to a single phase of filling with a locally undissolved matrix (Figure 6g) and thus do not allow for effective accommodation. Therefore, structural fractures do not significantly contribute to the reservoirs in the study area.

Dissolution fractures form due to the dissolution and enlargement of early structural fractures by fluids. Dissolution fractures are characterized by uneven fracture walls, uneven fracture widths, and unfilled interiors (Figure 6h). Their presence can often improve local connectivity but contributes less to the reservoirs themselves due to the limited scale of their development.

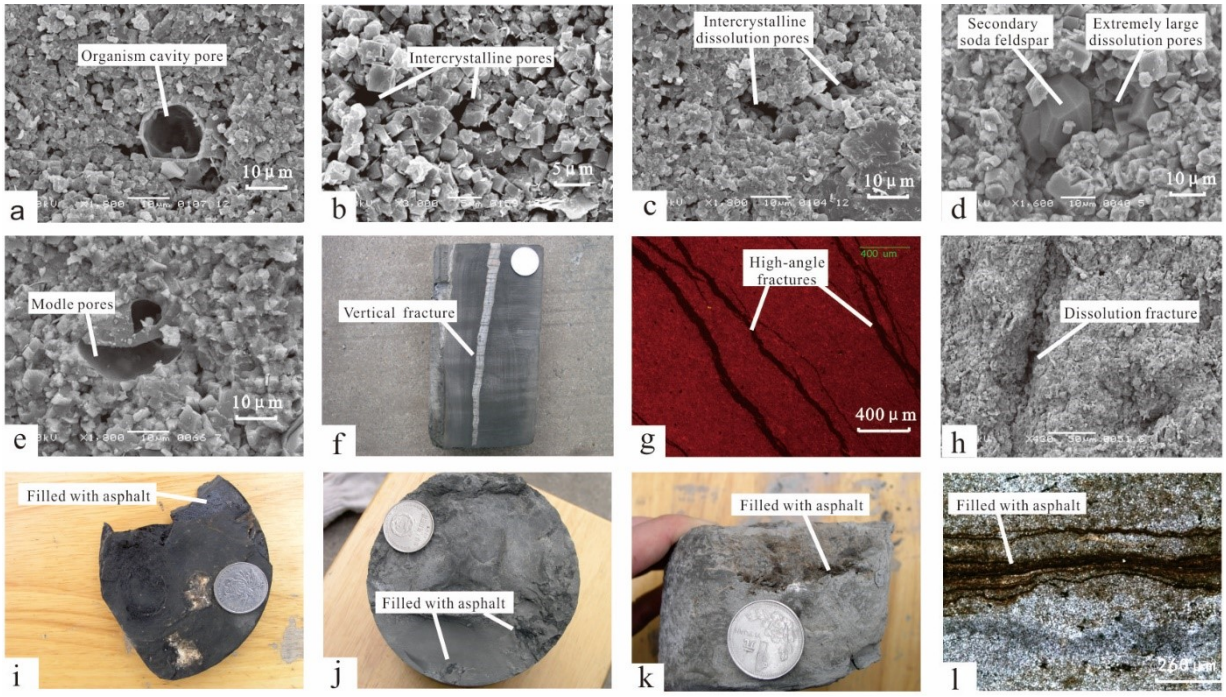

Figure 6: Accommodation types and characteristics of the dolomite reservoirs in Unit II of the LXF
a: algae organism cavity pores, X521, 1055.3 m, II 5, SEM; b: intercrystalline pores arranged in irregular polyhedrons, X521, 1042.5 m, II 5, SEM; c: intercrystalline dissolution pores, X521, 1055.3 m, II 5, SEM; d: extremely large dissolution pores internally filled with secondary sodium feldspar and micritic dolomite, XX1171, 785.6 m, II 1+2, SEM; e: mold pores resulting from the selective dissolution of organism cavity pores, XX461, 1295.5 m, II 1+2, SEM; f: vertical fractures completely filled with gypsum, X391, 1458.6 m, II 5; g: directional high-angle fractures completely filled with gypsum, within dolomite groups, nonluminescence, XX461, 1295.6 m, II 1+2, CL; h: dissolution fractures with irregular edges and uneven widths, XX461, 1388 m, II 5, SEM; i: obvious oil intrusion into the sandy dolomicrite of a sublayer in Unit II 3+4 of the LXF in well 391, with pores filled with asphalt, 1426 m; j: pores in the dolomicrite of a sublayer in Unit II 3+4 of the LXF in well 521 filled with asphalt, 1011.4 m; k: pores in the dolomicrite of a sublayer in Unit II 3+4 of the LXF in well 461 filled with asphalt, 1336.4 m; l: pores in the dolomicrite of a sublayer in lower Unit II 3+4 in well Xinxie 461 filled with asphalt, 815.9 m, plane-polarized light

The bulk of the gypsum nodules and crystals that developed in the lacustrine dolomicrite rocks within the study area were not corroded to form dissolution pores during late diagenesis. However, many studies of Paleozoic marine dolomite indicate that the dolomite rocks containing gypsum crystals and nodules were deposited in a specific environment, which provides a basis for the development of the reservoirs. The degree of gypsum corrosion during epidiagenesis and burial diagenesis is a major factor controlling the formation of good reservoirs [22]. The difference between inland shallow-buried lacustrine dolomite and deeply buried marine dolomite reflects their distinct mechanisms of reservoir formation.

5.2.2 Petrophysical characteristics of the dolomite reservoirs

To further investigate the properties of the various types of dolomite reservoirs and their differences, 29 core plug samples from well Xin 391 were selected for porosity and permeability tests and statistical analyses (Table 1).

In summary, the dolomicrite and sandy dolomicrite are petrophysically similar and are indicative of medium-porosity, super-low permeability reservoirs. The porosities of these dolomicrites range from 15%–25%. The muddy dolomicrite has the poorest petrophysical properties, with a predominant porosity range of 10%–15%, indicative of low-porosity, extra-low permeability reservoirs (Table 1). The dolomicrite and sandy dolomicrite mainly developed in the open lacustrine sedimentary environment, which indicates that the reservoirs from this facies belt have the best petrophysical properties. The dolomite reservoirs in the study area have a consistent relationship between porosity and permeability, *i.e.*, the porosity increases with increasing permeability (Table 1), indicating good pore structure near the reservoirs and well-connected pore networks.

Sample No.	Rock type	Depth(m)	Horizon	Minerals and their contents obtained by X-ray diffraction analys is					Porosity (%)	Permeability (md)	Median pore throat radius (nm)
				Calcite	Dolomite	Quartz+Feldspar	others	clay			
1	Sandy dolomicrite	1383.51	II 1+2	0.0	66.9	18.7	8.3	6.1	16.5	0.077	—
2	Dolomicrite	1384.03	II 1+2	0.0	69.5	9.3	14.6	6.6	15.8	0.094	—
3	Sandy dolomicrite	1385.18	II 1+2	0.0	51.4	10.8	35.2	2.6	24.9	1.160	—
4	Sandy dolomicrite	1385.28	II 1+2	0.0	68.3	16.4	5.4	9.9	20.1	0.280	96.500
5	Dolomicrite	1387.07	II 1+2	0.0	89.7	4.9	1.8	3.6	14.0	0.401	193.500
6	Dolomicrite	1389.50	II 1+2	0.0	81.5	8.4	5.0	5.1	20.2	0.091	98.100
7	Sandy dolomicrite	1393.15	II 1+2	0.0	60.5	22.4	3.2	13.9	27.6	0.709	197.600
8	Sandy dolomicrite	1397.46	II 1+2	0.0	81.6	11.3	0.0	7.1	17.0	0.097	38.100
9	Muddy dolomicrite	1397.61	II 1+2	0.0	50.6	11.9	24.9	12.6	14.2	0.082	31.700
10	Muddy dolomicrite	1406.81	Upper mudstone	0.0	42.0	19.2	12.1	26.7	7.9	0.017	—
11	Muddy dolomicrite	1409.66	Upper mudstone	0.0	41.1	22.4	10.4	26.1	0.7	0.088	—
12	Muddy dolomicrite	1424.89	II 3+4	0.0	67.7	13.1	2.8	16.4	7.6	0.053	5.800
13	Muddy dolomicrite	1430.89	II 3+4	2.5	71.8	9.7	3.5	12.5	13.4	0.039	0.039
14	Sandy dolomicrite	1433.57	II 3+4	1.6	56.2	27.3	4.7	10.2	16.2	0.150	0.150
15	Sandy dolomicrite	1435.01	II 3+4	0.0	72.1	12.4	7.6	7.9	20.3	0.231	109.400
16	Muddy dolomicrite	1440.46	Lower mudstone	3.2	56.1	10.7	2.8	27.2	16.6	0.044	25.400
17	Dolomicrite	1455.28	II 5	0.0	80.7	8.0	5.0	6.3	14.9	0.151	0.151
18	Sandy dolomicrite	1456.77	II 5	0.0	68.5	18.4	5.5	7.6	12.8	0.051	21.900
19	Sandy dolomicrite	1456.99	II 5	1.2	64.6	13.8	10.6	9.8	17.1	0.443	0.443
20	Dolomicrite	1457.54	II 5	0.0	86.7	6.0	1.6	5.7	16.8	0.138	98.800
21	Dolomicrite	1458.82	II 5	0.0	80.8	8.6	3.6	7.0	16.2	0.284	131.700
22	Dolomicrite	1459.14	II 5	0.0	84.1	9.8	1.6	4.5	16.7	0.269	203.400
23	Dolomicrite	1459.39	II 5	0.0	84.7	9.6	0.0	5.7	18.5	0.127	0.127
24	Dolomicrite	1461.17	II 5	0.0	83.1	9.4	2.3	5.2	19.6	0.149	129.700
25	Dolomicrite	1462.71	II 5	0.0	67.4	8.7	19.9	4.0	16.3	0.142	0.142
26	Dolomicrite	1467.57	II 5	0.0	79.7	9.1	2.6	8.6	17.4	0.183	0.183
27	Muddy dolomicrite	1469.79	II 5	0.0	60.5	14.2	9.2	16.1	12.6	0.073	0.073
28	Dolomicrite	1474.45	II 5	0.0	86.2	8.6	0.9	4.3	15.7	0.833	174.000
29	Sandy dolomicrite	1477.78	II 5	2.9	74.6	12.3	1.6	8.6	16.5	0.056	0.056

Table 1: X-ray diffraction and petrophysical analysis results for the samples from the dolomite reservoirs of LXF Unit II in well Xin 391

5.2.3 Pore throat textural characteristics of the dolomite reservoirs

The mercury injection data for well Xin 391 indicate that three types of dolomite reservoirs exist in the study area. The pore throat radii of these reservoirs are mainly nanometer-scale pore throats. The dolomicrite and sandy dolomicrite have similar pore throat radii, which mostly range from 0–2 nm and 50–250 nm, respectively, with maximum respective values of 203 nm and 197.6 nm. The muddy dolomicrite has much lower values than both the dolomicrite and the sandy dolomicrite. With pore throat radii of < 50 nm and a maximum pore throat radius as low as 31.7 nm (Table 1), the muddy dolomicrite has poorer pore connectivity. This may be due to one of two factors: (1) the development of clay minerals that allow masses of silky, flaky illite to fill the intercrystalline spaces and to block the pores and decrease the pore throat radii; or (2) an increase in the clay mineral content that leads to the development of organic and interbedded pores in the clay minerals, which also impacts the distribution range of the pore throat radii.

5.3 Model for the co-occurrence of dolomicrite and dark argillite and its implications

During the deposition of Unit II of the LXF in the Qianjiang Depression, the water level fluctuated rapidly and frequently, resulting in the co-occurrence of interbedded dark argillite and dolomite [17]. In previous research, the source rock, reservoirs, and hydrocarbon accumulations of the study area were discussed independently [15, 23**?**]. Few studies, however, have addressed the petroleum geology implications of source-reservoir co-occurrence. This investigation fills this gap by considering the hydrocarbon-generating potential of the interbedded dark mudstones and the impact of the dark mudstone formation environment upon the petrophysical properties of the dolomite reservoir by developing a model for hydrocarbon accumulation.

5.3.1 Good hydrocarbon-generation potential in the well-developed dolomite intervals

Studies of the hydrocarbon-generation potential of source rock in continental salt lakes provide evidence of source rocks that generate large volumes of hydrocarbons, even if they contain small volumes of organic matter (*e.g.*, TOC of

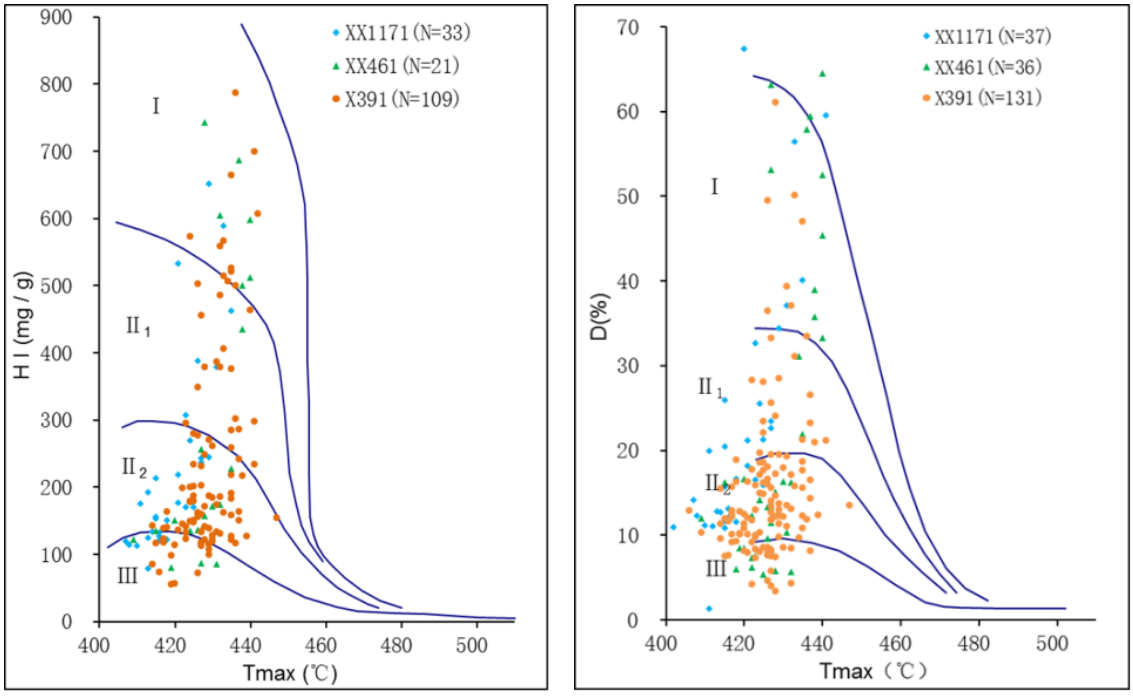

Figure 7: HI-Tmax and D-Tmax plots for the source rock of LXF Unit II in the study area

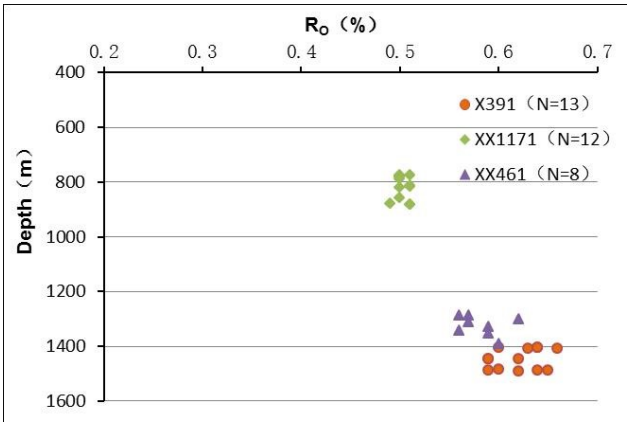

Figure 8: Plot of R_o vs. depth for the source rock of LXF Unit II in the study area

> 0.6%) and are in an early evolutionary stage [24, 25]. This conclusion somewhat lowers the criterion for source rock evaluations in continental salt lakes compared to conventional lakes [26, 27].

The dark argillite interbedded with dolomicrite in Unit II of the LXF in the study area is a configuration that is mainly present in the productive zones of Units II 5, II 3+4, and II 1+2 of the LXF. The correct nouns have TOC values that range from 0.5%–2% (average 1.29%), indicating medium to good source rock [28–30], with some samples constituting excellent source rock based on the fact that their TOC values are > 4% (Figure 4). In the overlying and underlying mudstones, however, the dolomites are poorly developed, with TOC values generally < 0.5% (Figure 4), which is indicative of poor source rock [31, 32]. The primary unit has organic type II_2, and there are small amounts of types II_1 and III (Figures 7 and 9). The source rocks have vitrinite reflectance values of 0.5%–0.7% (average 0.57%) (Figure 8), which falls within the thermal maturity range of immature to early oil generation [33, 34]. Sporopollen and algae are visible under plane-polarized light and are light yellow under fluorescence microscopy (Figure 9). Their presence is indicative of an immature thermal evolutionary stage [17, 35, 36]. In summary, the organic-rich dark argillite rocks interbedded with dolomicrite rocks have great potential for the generation of immature hydrocarbons.

5.3.2 The developmental environment of dark argillite can improve the petrophysical properties of reservoirs

Davies [37] suggested that the depositional environment of dark argillite combined with its organic evolution can supply CO_3^{2-} ions much more easily than other environments suitable for dolomite formation. Through experiments, Baker and Kastner [38] concluded that low concentrations of SO_4^{2-} ions, rather than high concentrations of Mg^{2+} and Ca^{2+} ions, in dolomitization fluids are crucial

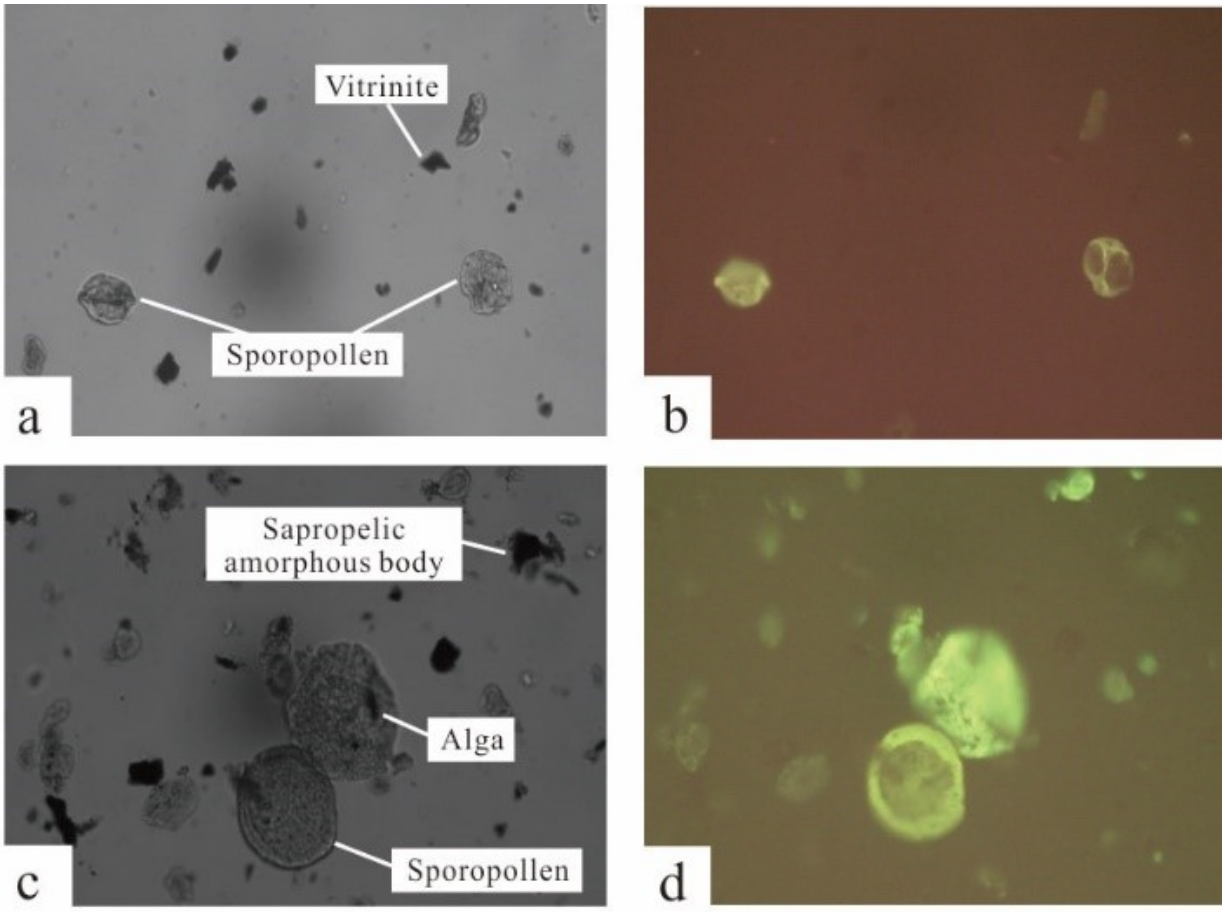

Figure 9: SEM characteristics of the kerogen in Unit II of the LXF in well Xinxie 1171
a: sporopollen and vitrinite under SEM, sublayers of Unit II 1+2 of the LXF, 780.2 m, plane-polarized light, ×40; b: light yellow-colored sporopollen under SEM, under fluorescence; c: sporopollen, algal, and sapropelic amorphous bodies, sublayer of Unit II 5 of the LXF, 884.6 m, plane-polarized light, ×40; d: light yellow-colored sporopollen, algae under SEM, under fluorescent lighting

for dolomite formation. In the study area, the dark mudstones are intercalated with many gypsum veins and nodules, and the precipitation of gypsum leads to a certain decrease in the SO_4^{2-} concentration of the solution and the eventual formation of dolomite. Mansfield [39] proposed that in environments in which dark argillite is formed, organic matter and organic compounds are abundant and can accelerate dolomite formation. Maehel and Mountjoy [40] proposed that dark argillite is generally formed in alkaline environments favorable for dolomite formation.

In summary, the formation environment of dark argillite along with its organic evolution can often boost the formation of the co-occurring dolomite, which is capable of being completely dolomitized. In addition, early dolomitization can often increase the pore volume and compression resistance of pores [41] and can improve the petrophysical properties of a reservoir. Dolomitization results in positive changes to the petrophysical properties of the reservoir, especially the dolomite reservoirs in the study area, which underwent single-phase dolomitization and were less impacted by later diagenesis.

5.3.3 Model for hydrocarbon accumulation within source rock

In the study area, the three reservoirs in Unit II of the LXF are characterized by the occurrence of interbedded dolomicrite and organic-rich dark argillite. The establishment of such a special source-reservoir co-occurrence model provides important guidance for evaluating the physical properties of the region of interest. For example, correlations between the oil and source materials of Unit II match the model.

The properties of Xingou crude oil are distinct from those of oil in the adjoining Laoxin and Tuoshi Regions. The Laoxin and Tuoshi Oilfields are located north of the Xingou Oilfield. These three oilfields represent the main

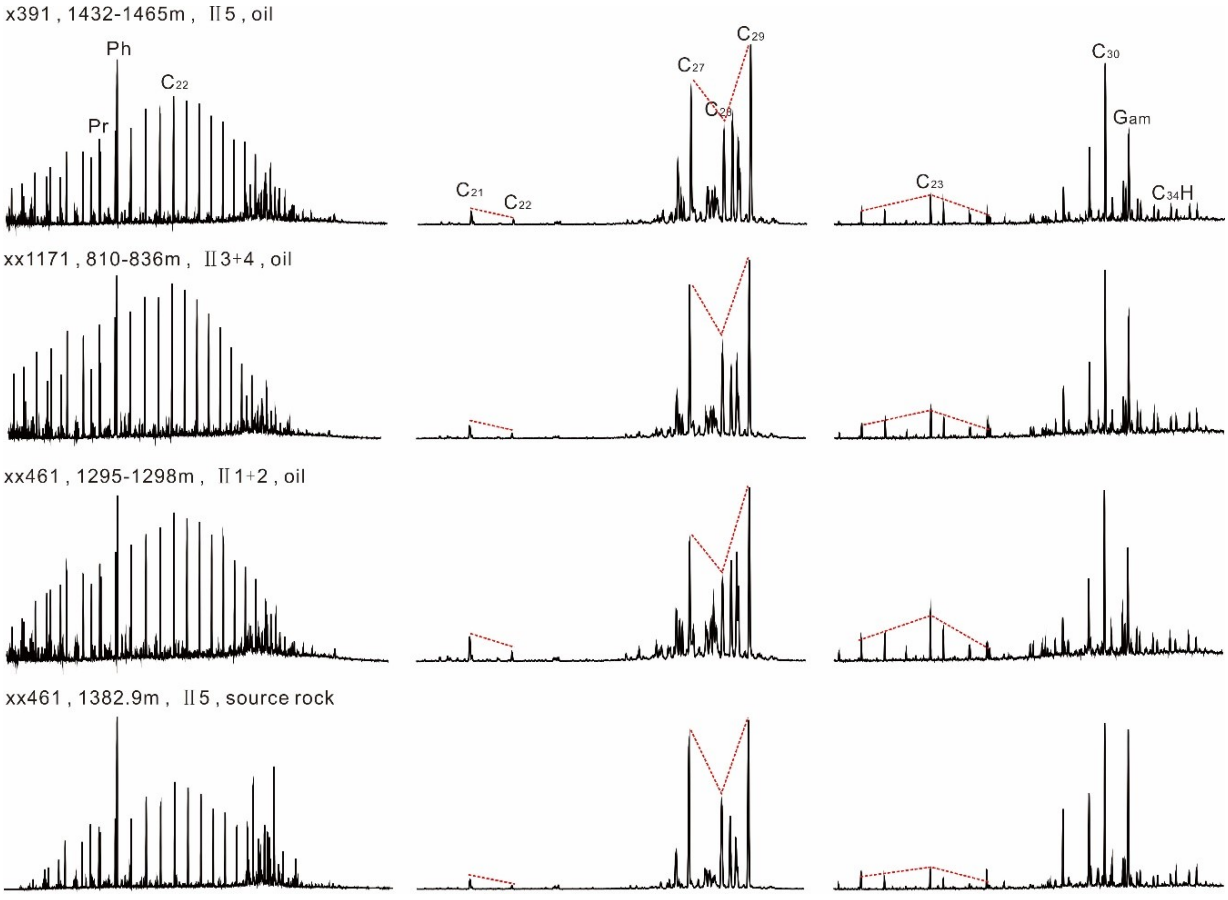

Figure 10: Oil-source correlation for Unit II of the LXF in terms of characteristics of the biomarker compounds sterane and terpane

oil producers in the Qianjiang Depression. Their crude oil is sourced from the Zongkou Syncline, which is a main hydrocarbon-generating depression within the Qianjiang Depression (Figure 2). Laoxin and Tuoshi oils have average oil densities of approximately 0.8111 g/m^3 and 0.8169 g/m^3, respectively, and average respective viscosities of 4.10 and 4.46 mPa·s, values that are indicative of light oil. In contrast, Xingou oil has an average density of 0.8658 g/cm^3 and a viscosity of 20.26 mPa·s, which is indicative of heavy oil, and its saturation is lower than that of the Laoxin and Tuoshi oils [42]. These differences indicate that the source of the Xingou crude oil differs from that of the Laoxin and Tuoshi oils.

The biomarker compounds in the source rock and oil of Unit II of the LXF have similar distributions. The n-alkanes of the 3 crude oil samples and 1 source rock sample from Unit II of the LXF exhibit single peak values, which include a main peak (post-peak) related to C_{22}. In the oil and mudstone samples, the isoprenoid alkene series values are high, with a Pr/Ph ratio < 1 (Figure 10), indicating that both the crude oil and the source rock formed in reducing environments. For the relative compositions of the normal steranes C_{27}, C_{28}, and C_{29}, both the crude oil and the source rock of Unit II of the LXF show a C_{29}20R > C_{27}20R > C_{28}20R distribution. Similarly, the correct noun forms a backwards "L" shape. The crude oil samples have $C_{27}\alpha\alpha\alpha$20R/$C_{29}\alpha\alpha\alpha$20R ratios of 0.60–0.70, which average 0.70 and 0.80 for the source rock samples, respectively (Figure 10), indicating that both were formed in strongly reducing, saline, lacustrine environments [43]. For the maturity parameter, the crude oil has C_{29}20S/(20S+20R) ratios of 0.32–0.40, compared with 0.23 for the source rock (Figure 11), indicating that both are immature.

The oil-source correlation results indicate that the source-reservoir interbedding is characteristic of self-sourced reservoirs. The open lacustrine subfacies is a favorable unit for hydrocarbon accumulation in the study area.

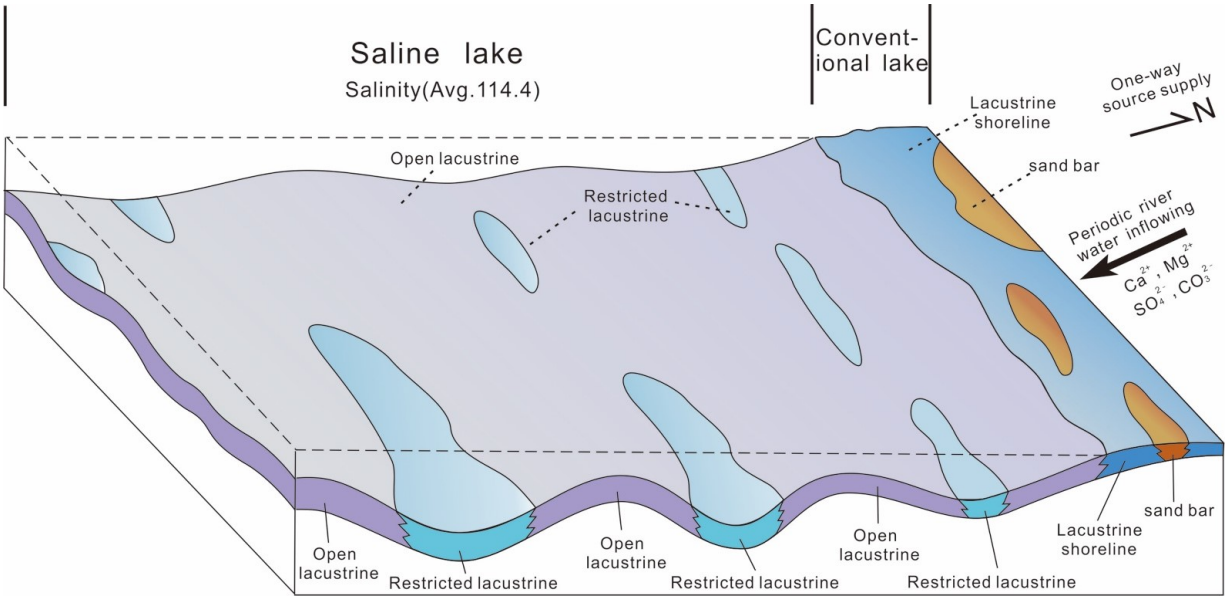

Figure 11: Sedimentary model for dolomicrites in Unit II of the LXF in the Xingou Region

6 Discussion

6.1 Lateral distribution of lacustrine dolomite and its controlling factors

Previous interpretations of the Xingouzui Formation suggest that this unit consists of lacustrine deposits that accumulated in an arid to semi-arid climate [42, 44, 45]. A deltaic-normal, lake-brine lake sedimentary system is thought to have developed in the Qianjiang Depression, which was affected by the Hanchuan sediment provenance region to the northeast of the depression and the Hanshui sediment provenance region to the northwest (Figure 2). The limited provenances to the west and south exerted less influence on the sedimentary environment [44–46]. This asymmetrical supply pattern resulted in large sedimentary differences between the southern and northern areas of the Qianjiang Depression. The central and northern areas were affected by mechanical forces and had low salinities (averaging 9.84%) due to the presence of a fluvial system. In these areas, terrigenous detrital deposits were dominant. Since the southern area is far from the main provenance areas in the north, this region was dominated by chemical forces, and had high salinities (averaging 12.4%ffl) due to its confined water environment (Figure 11).

In the study area, the lateral distribution of Unit II of the LXF sedimentary facies should be studied in detail using single-well analyses and well correlations, and its seismic attributes should be predicted. In the diagram summarizing the seismic attributes of Unit II of the LXF, increased amplitude values are shown in purple-red, blue, and green (Figure 5), with the blue and green areas corresponding to the highest-amplitude areas found in the Laoxin region, which is in the northern part of the study area and is adjacent to the provenance region. In the high-amplitude areas, interbedded sandstone-mudstone is dominant, indicating a sandbar-dominated sedimentary environment. In the study area, interbedded carbonate-mudstone is dominant and corresponds to the moderate- to high-amplitude areas, which are shown in blue with a few purple-red streaks, indicating an open lacustrine environment. In the plot of the average reflection strength attribute, the restricted lacustrine subfacies exhibits weak reflection signatures (purple-red areas). These regions occur in depressions and indicate an argillaceous low-sedimentary environment. The distributions of the various types of subfacies are characterized by drops in the lake level, which allowed the lake basin area to continuously shrink from Units II 5 to II 1+2 of the LXF. These drops in lake level favored an increasing area of open lacustrine subfacies in the favorable reservoir facies belt and a decreasing argillaceous low-sedimentary area. The various subfacies are laterally distributed in a ring pattern, which displays a northwest-southeast transition from a lacustrine shoreline to open lacustrine and then to restricted lacustrine (Figures 5 and 11).

Based on our analysis of the stratigraphic occurrence of dolomite and the lateral distribution of the sedimentary facies, we conclude that the development and distribution

of lacustrine carbonate rocks in the study area were controlled by provenance, lake level fluctuations, and paleogeomorphologic changes.

Control of the paleo-provenance system over the distribution of lacustrine carbonates: Lacustrine carbonates are generally deposited in shallow water areas, which are located opposite a delta and away from the provenance regions [47–50]. Due to less provenance influence, the lake waters in these areas have high salinities that are favorable for the deposition of carbonates, whereas in the shallow water areas adjacent to the deltaic deposits, carbonates are poorly developed due to the high-energy, low concentration conditions resulting from greater provenance influence. Therefore, alternative deposits such as shallow-lake sandbars and shallow-lake muds are dominant. The facies transition from lower Unit II 5 of the LXF to lower Unit II 1+2 of the LXF indicates that the shrinkage of the deltaic and shallow-lake sandbar areas resulted in the enlargement of the carbonate distribution area, *i.e.*, both show contact relationships, in which entity *A* decreases and entity *B* increases.

The control of paleo-microgeomorphology over the distribution of favorable carbonate reservoir facies zones: Relative paleogeomorphologic analysis (via the restoration of stratigraphic thicknesses) of the individual units before and after deposition indicates that in the very thick, low terrains, argillite with either several gypsum beds or a few thin-bedded muddy dolomicrites or gypsiferous dolomicrite are dominant, and carbonates are not generally present. In thin, high terrains, interbedded dolomicrite or dark argillite are dominant, constituting a good source-reservoir association and representing a favorable reservoir facies belt in the study area [17].

The control of lake level fluctuation over vertical intervals and the frequency of lacustrine carbonates: Analysis of the stratigraphic sequence of the four well cores in the study area (Figures 2 and 4) indicates that the vertical distribution of the lacustrine carbonates was primarily controlled by lake level fluctuations, *i.e.*, during the early stage of a transgression or the late stage of a regression of the lake water, the lake basin subsided slowly and was moderately charged. At that time, the lake water was shallow and highly saline, which was favorable for carbonate deposition in an open lacustrine sedimentary environment [51, 52]. During the late stage of a transgression or the early stage of a regression of the lake water, the basin was undercharged with deep water, which was unfavorable for carbonate deposition. At that time, dark argillite deposits were dominant. Shen *et al.* [42] concluded that the fluctuation of the lake level in the Jianghan Basin was rapid and frequent during the deposition of Unit II of the LXF. This would also result in the frequently interbedded dolomicrite-mudstone observed in the study area.

6.2 Formation mechanisms of dolomite reservoirs

The dolomites of Unit II of the LXF have a fine-grained micritic texture. Previous studies have consistently considered these dolomites to be regional source or cap rocks [15]. However, more recent studies indicate that despite being tight, the dolomicrite in the study area has a certain reservoir potential due to its medium-porosity and extremely low permeability [17]. Previous studies have neglected to examine how these micritic texture dolomite reservoirs preserve their pores so perfectly to maintain medium porosities. Therefore, in this study, the mechanism for the formation of dolomicrite reservoirs is discussed in terms of diagenesis, dolomitization, and hydrocarbon charging.

The dolomite reservoirs were formed during diagenesis, which is characterized by weak compaction and good preservation of intercrystalline pores. The Paleocene Unit II of the LXF was buried at approximately 1000 m in a shallow to moderately deep diagenetic environment. In this environment, the dolomite reservoirs have a dolomicrite texture with rough, crystalline surfaces and xenotopic crystals with few dissolution pores and fractures. The interbedded dark argillite in this unit has vitrinite reflectance values in the range of 0.4%–0.6%, which is indicative of immature source rock that has generated immature oil. This suite of characteristics indicates that the dolomite reservoirs in the study area were formed during an early diagenetic stage. During this time, the reservoirs were less influenced by diagenesis. This resulted in the perfect preservation of the intercrystalline pores due to weak compaction, which decreased porosity and dissolution while increasing porosity. With increasing diagenesis, the micritic-textured dolomite reservoirs have difficulty achieving medium porosity. For example, in the Bohai Bay Basin, the Paleogene member of the Sha III lacustrine dolomicrite and the micritic dolomite were formed during interim diagenesis. At that time, dissolution pores were dominant in the reservoirs and ranged from 5%–15%, as the intense compaction was unfavorable for preservation in intercrystalline pores. Therefore, these reservoirs have extremely low to low porosities [16]. In the Tarim Basin, the Cambrian-Ordovician marine dolomicrite was formed during late stage intensive diagenesis. Crystals intimately contact each other, with an average porosity of 0.55% [53], much lower than that in the study area.

Intensive dolomitization enlarges intercrystalline pores and increases intercrystalline compression resistance. The extensive micritic-textural dolomites were formed as a result of later dolomitization of the backflow infiltration, rather than primary precipitation [17]. In the dolomites, calcite content is generally as low as < 3%. Most of the samples that do not contain calcite (Table 1) are indicative of intensive dolomitization in the study area. Morrow [41] proposed that the complete replacement of calcareous sediments by dolomite can decrease reservoir volume by 6%–13%, with intercrystalline porosity increasing accordingly. The dolomites in the study area were subjected to diagenesis at an early time, which resulted in negligible destruction of the intercrystalline pores by later recrystallization efforts. Moreover, the dolomites that formed due to dolomitization provide a sound supporting framework and are more compression- and dissolution-resistant than limestones, thus making them favorable for the preservation of intercrystalline pores [54, 55].

Charging of hydrocarbons in dolomite reservoirs can prevent cementation and boost the preservation of intercrystalline pores. In the Qianjiang Depression, the extensive hydrocarbon generation and charging system was mainly established at the end of the deposition of the Jinghezhen Formation (Figure 2). The dolomite reservoirs in the Xingou Region were charged by hydrocarbons during this period, and exhibit secondary grayish-yellow to medium brown colors (Figures 4 and 6). Previous research addressed the fact that the presence of hydrocarbons in carbonate fluids inhibits the transmission of ions such as Ca^{2+}, Mg^{2+}, and CO_3^{2-}, which further results in poor cementation of the existing pore spaces. In addition, during later burial diagenesis, the asphalt cap (transformed from oil) over the pore walls (Figures 6i, j, k, and l) could also inhibit precipitation of the cement [56–58]. Both of these factors provide favorable conditions for preserving intercrystalline pores.

7 Conclusions

(1) In Unit II of the LXF in the Xingou Region, the dolomites can be divided into dolomicrite, muddy dolomicrite, sandy dolomicrite, and gypsiferous dolomicrite, of which dolomicrite is the most developed. The dolomicrite is characterized by anhedral crystals with rough crystalline surfaces and non-embedded contacts. The dolomicrites formed in shallow water, evaporative sedimentary environments.

(2) Unit II of the LXF contains open lacustrine, restricted lacustrine, and lacustrine shoreline subfacies. Of these subfacies, the open lacustrine subfacies developed primarily in the shallow lake area with a relatively high topography. This subfacies is extensive throughout the study area. The restricted lacustrine subfacies occurs in topographically low lake bottom areas. The lacustrine shoreline subfacies is rare and is only found on the northeast margin of the study area. The spatial distributions of these subfacies are controlled by the paleo-provenance system, the paleomicrogeomorphology, and lake level fluctuations. From the lake basin margin to the center of the lake, a facies transition series occurs from lacustrine shoreline to open lacustrine to restricted lacustrine.

(3) Of the three types of dolomite reservoirs examined in this study, secondary intercrystalline pores are dominant within the spatial reservoir types. The petrophysical properties of the dolomicrite are most similar to those of the sandy dolomicrite. Both constitute medium-porosity, low-permeability reservoirs deposited in open lacustrine environments. The muddy dolomite reservoirs possess the poorest petrophysical properties, as they were deposited in a restricted lacustrine environment. The three types of dolomite reservoirs have porosities that are related to their permeabilities, *i.e.*, their porosities increase with increasing permeability, which is indicative of good pore structure.

(4) In the study area, the formation of dolomicrite and structural dolomite reservoirs is controlled by three factors. First, the dolomite reservoirs were all formed during early diagenesis, during which the intercrystalline pores were well preserved due to shallow burial and weak compaction. Second, post-sedimentary intensive dolomitization increased the intercrystalline porosities. In addition, the newly formed dolomites were more compression- and dissolution-resistant, which favors the preservation of intercrystalline porosities. Finally, hydrocarbon charging in the dolomite reservoirs can hamper cementation during later diagenesis, which favors the preservation of intercrystalline pores.

(5) In the interbedded layers of the dolomite reservoir rocks and the dark argillite of Unit II of the LXF, the argillite rocks contain a high abundance of organic matter, with suitable organic types and low maturities that can generate large volumes of immature oil. Their formation environment and organic evolution can improve the petrophysical quality of the

dolomite reservoirs. Oils from the three productive intervals were self-sourced from the immature rocks within the formation. Therefore, it can be inferred that the open lacustrine subfacies represents a favorable depositional facies for hydrocarbon accumulation in the study area.

Acknowledgement: This study was supported by the Open Fund of the Key Laboratory of Exploration Technologies for Oil and Gas Resources (Yangtze University), Ministry of Education (Grant No. K2017-02), and the Natural Science Foundation of Hubei Province (Grant No. 2016CFB601). We would like to thank Dr. Junjie Chang and Jun Cai for their valuable suggestions during the preparation of the manuscript. We also thank the Exploration and Development Research Institute of Jianghan Oilfield Co., Ltd. for data support. In addition, we appreciate the editors and reviewers for their critical and helpful comments and suggestions.

References

[1] Xia Q.S., Tian J.C., Ni, X.F., Lacustrine carbonate rocks in china: an overview. Sedimentary Geology and Tethyan Geology, 2003, 23, 105-112 (in Chinese with English abstract).

[2] Li C., Genesis and reservoir characteristics of lacustrine dolomite in the lower part of the sha-1 formation in qikou depression. PhD thesis, China University of Petroleum (EastChina), China, 2011, 80-100.

[3] Liu J.Q., Liu R., Chen H.H., Study on sedimentary facies types and spatial distribution in $H_3$of biyang depression. Petroleum Geology and Engineering, 2010, 24, 1-4 (in Chinese with English abstract).

[4] Pan T., Sequence straigraphy & sedimentary features analysis of lacustrine carbonate rock in upper 4^{th} member of shahejie formation, shaojia area, zhanhua depression. PhD thesis, China University of Geosciences, Wu Han, China, 2011, 70-80.

[5] Sun Y., Zhong J.H., Yuan X.C., Genesis of the dolostones from the first member of the shahejie formation in the huimin depression, shandong. Sedimentary Geology and Tethyan Geology, 2007, 27, 78-84 (in Chinese with English abstract).

[6] Wang H.L., Gao X.Z., Yang D.X., Hao L.I., Zhang Z.Y., Genesis of dolomitic rock within the lower cretaceous lacustrine facies in bayindulan sag, erlian basin. Acta Sedimentologica, 2014, 32, 560-567 (in Chinese with English abstract).

[7] Qi Z.X., Shu X.W., Sang L., Zhang Y.S., The forming pattern of intersalt argillaceous dolomite in qianjing formation of qianjiang depression. Journal of Yangtze University, 2012, 9, 19-32 (in Chinese with English abstract).

[8] Xian B.Z., Jiang Z.X., Gao F.Z., Sedimentary Systems in the Member 2 of Hetaoyuan Formation of Paleogene in Biyang Depression of Henan Province. Journal of Palaeogeography, 2002, 4, 31-37 (in Chinese with English abstract).

[9] Zhang Y., Yang Y., Qi Z., Sedimentary characteristics and environments of the salt-bearing series of qiangjiang formation of the paleogene in qianjiang sag, jianghan basin. Journal of Palaeogeography, 2003, 5, 29-35. (in Chinese with English abstract).

[10] Jiao C.L., Xing X.J., He B.Z., Chen D.Z., Li C.C., Characteristics and genetic types of cambrian-ordovician dolomite reservoirs in tarim basin. Geology in China, 2011, 38, 1008-1015 (in Chinese with English abstract).

[11] Pan L.Y., Liu Z.G., Li C., Shou J.F., Zhang J.Y., Dolomitization and its relationship with reservoir development of the lower triassic feixianguan formation in eastern sichuan basin. Journal of Palaeogeography, 2012, 14, 176-186 (in Chinese with English abstract).

[12] Wu S.Q., Qian Y.X., Li H.L., Yang S., Sha X., Characteristics and main controlling factors of dolostone reservoir of the middle-lower ordovician yingshan formation in katak uplift of tarim basin. Journal of Palaeogeography, 2012, 14, 209-218 (in Chinese with English abstract).

[13] Zhang J., Hu J., Luo P., Song J., Master control factors of deep high-quality dolomite reservoirs and the exploration significance. Petroleum Exploration and Development, 2010, 37, 203-210. (in Chinese with English abstract).

[14] Zhao W.Z., Shen A.J., Zheng J.F., Qiao Z.F., Wang X.F., The porosity origin of dolostone reservoirs in the tarim, sichuan and ordos basins and its implication to reservoir prediction. Science China: Earth Sciences, 2014, 57, 2498-2511 (in Chinese with English abstract).

[15] Li Y.F., Xia S.M., Long Y.M., Featuer analysis of xingou argillaceous dolomite reservoir in jianghan basin. Journal of Jianghan Petroleum University of Staff and Workers, 2014, 27, 8-11 (in Chinese with English abstract).

[16] Qu C.W., Lin C.M., Cai M.J., Cheng Y., Wang B., Characteristics of dolostone reservior in sha 3 group from palaeogene shahejie formation in beitang sag, bohaiwan basin. Acta Geologica Sinica, 2014, 88, 1588-1602 (in Chinese with English abstract).

[17] Shen J.J., Mechanism for formation of lacustrine dolomites of the lower xingouzui formation in the Southern Part of the qianjiang depression and its petroleum geologic implication. PhD thesis, Yangtze University, Wuhan, China, 2015, 60-75.

[18] Lu M.G., Tong X.L., Wang B.J., Analysis of reservior formation periods, the jiangling depression of the jianghan basin. Petroleum Geology and Experiment, 2004, 26, 28-30 (in Chinese with English abstract).

[19] Fang Z.X., Hydrocarbon Exploration Signification of Intersalt Sediments in Qianjiang Saline Lake Basin. Acta Sedimentologica Sinica, 2002, 20, 608-620 (in Chinese with English abstract).

[20] Dunham R.J., Classification of Carbonate Rocks According to Depositional Texture. In: Classification of Carbonate Rocks Symposium. American Association of Petroleum Geologists, Tulsa, 1962, Memoir 1, 108-121.

[21] Feng Z.Z., Sedimentary Petrology. Beijing: Petroleum Industry Press, Beijing, 1993, 104-135.

[22] He J., Zhang Z.J., Qiao L., Wei W., Wang Y., Occurrence, genesis and evolution of evaporite minerals in dolomite reservoir: a case study of the majiagou formation in gas fields of the central ordos basin. Oil and Gas Geology, 2013, 34, 659-666 (in Chinese with English abstract).

[23] Hu Y., Lu S.F., Li W.H., Xue H., Zhang P., Oil-bearing property analysis of argillaceous dolomite in xingouzui formation in the jianghan basin. Journal of Northeast Petroleum University, 2015,

39, 76-81 (in Chinese with English abstract).
[24] Bao J.P., The study of immature and low-mature oil in salt-lake basin. Geological Publishing House Press, Beijing, 2006, 196-204.
[25] Wang T.G., Genetic mechanism and occurrence of immature hydrocarbon. Beijing: Petroleum Industry Press, Beijing, 1995, 121-125.
[26] Espitalié J., Marquis F., Sage L., Organic geochemistry of the Paris Basin, in: Brooks, J., Glennie, K. (Eds.), Petroleum Geology of Northwest Europe. Graham and Totman, London, 1987, 1, 71-86.
[27] Peters K.E., Guidelines for evaluating petroleum source rock using programmed pyrolysis. AAPG Bulletin, 1986, 70, 318-386.
[28] Lafargue E., Espitalié J., Marquis F., Pillot D., Rock Eval 6 applications in hydrocarbon exploration, production, and soil contamination studies. Inst. Fr. Pet., 1998, 53, 421-437.
[29] Mendhe V. A., Mishra S., Kamble A.D., Varma A.K., Bannerjee M., Varade A.M., Kumar S., Geological controls and flow mechanism of Permian shale gas reservoir of Raniganj Basin, West Bengal, India. J. Geosci. Res., 2017c, 1, 161-172.
[30] Peters K.E., Cassa M.R., Applied source rock geochemistry, in: Magoon, L.B., Dow, W.G. (Eds.), The Petroleum System from Source to Trap. AAPG Bulletin, 1994, 60, 93-120.
[31] Mendhe V.A., Mishra S., Khangar R.G., Kamble A.D., Kumar D., Verma A.K., Singh H., Kumar S., Bannerjee M., Organopetrographic and pore facets of Permian shale beds of Jharia Basin with implication to shale gas reservoir. J. Earth Sci., 2017d, 28, 897-916.
[32] Mendhe V. A., Kumar V., Saxena V.K., Bannerjee M., Kamble A.D., Singh B.D., Mishra S., Sharma S., Kumar J., Varma A.K., Mishra D.K., Samad, S.K., Evaluation of gas resource potentiality, geochemical and mineralogical characteristics of Permian shale beds of Latehar-Auranga Coalfield, India. Int. J. Coal Geol. 2018b, 196, 43-62.
[33] East J.A., Swezey C., Repetski J.E., Hayba D.O., Thermal maturity map of Devonian shale in the Illinois, Michigan, and Appalachian Basins of North America. U.S. Geological Survey Scientific Investigations, 2012, Map 3214, 1 sheet.
[34] Swezey C., Total Petroleum Systems of the Michigan Basin - Petroleum geology and geochemistry and assessment of undiscovered resources. U.S. Geological Survey Digital Data Series DDS-69-T, 2015, Chapter 2, 162.
[35] Swezey C., Hatch J., Brennan S., East J.A., Rowan E., Repetski J., Assessment of undiscovered oil and gas resources of the Illinois Basin, 2007. U.S. Geological Survey Fact Sheet, 2007, 3058, 2.
[36] Swezey C., Regional stratigraphy and petroleum systems of the Illinois Basin, U.S.A. U.S. Geological Survey Scientific Investigations Series Map, 2009, SIM-3068, 1 sheet.
[37] Davies P.J., Bubela B., Ferguson J., Simulation of carbonate diagenetic processes: formation of dolomite, hunrtiteand monahydrocalcite by the reactions between nesquehonite and brine. Chem. Geol., l977, 19, 187-214.
[38] Baker P.A., Kastner M., Constrairits on the formation of sedimentary dolomite. Science, l981, 213, 214.
[39] Mansfield C.F., A urolith of biogenic dolomite-another clue in the dolomite mystery. Geochimica Et Cosmochimica Acta, 1980, 44, 829-831.
[40] Maehel H.G., Mountjoy E.W., Chemistry and environments of dolomitization-a reappraisal. Earth-Science Reviews, 1986, 23, 175-222.
[41] Morrow D.W., The chemistry of dolomitization and dolomite precipitation. Geoscience Canada, 1982, 9, 5-13.
[42] Shen J.J., Chen B., Wang C.L., Song H.X., Zhou X.F., Sedimentary characteristics of gypsum-salt rocks in palaeogene shashi formation of jiangling depression. Acta Geoscientica Sinica, 2014, 35, 425-433 (in Chinese with English abstract).
[43] Taylor G.H., Teichmüller M., Davis A., Diessel C.F.K., Littke R., Robert P., Organic Petrology. Gerbrüder Borntraeger, Berlin. 1998, 16, 704.
[44] Guo H., Wu S.Q., Cao W.S., Zeng F., Yang W.T., Study on oil reservoir layer features in southeast of qianjiang sag in jianghan basin. Journal of East China Institute of Technology, 2007, 30, 231-235 (in Chinese with English abstract).
[45] Wang B.J., Lin C.S., Chen Y., Lu M.G., Liu J.Y., Episodic tectonic movement and evolutional character in jianghan basin. Oil Geophysical Prospecting, 2006, 41, 226-230 (in Chinese with English abstract).
[46] Hu Z.G., Hu M.Y., Hu J.Z., Liu D.M., Shallow water delta depositional model of the lower segment of the xingouzui formation in eastern qianjiang depression. Geology in China, 2011, 38, 1263-1273 (in Chinese with English abstract).
[47] Alonso-Zarza A.M., Zhao Z., Song C.H., Li J.J., Zhang J., Mudflat/distal fan and shallow lake sedimentation (upper Vallesian-Turolian) in the Tianshui Basin, Central China: Evidence against the late Miocene eolian loess. Sedimentary Geology, 2009, 222, 42-51.
[48] Anadón P., Utrilla R., Sedimentology and isotope geochemistry of lacustrine carbonates of the Oligocene Campins Basin, northeast Spain. Sedimentology, 2010, 40, 699-720.
[49] Burton D., Woolf K., Sullivan B., Lacustrine depositional environments in the Green River Formation, Uinta Basin: Expression in outcrop and wireline logs. AAPG Bulletin, 2014, 98, 1699-1715.
[50] Platt N.H., Lacustrine carbonates & pedogenesis: sedimentology and origin of palustrine deposits from the Early Cretaceous Rupelo Formation, W Cameros Basin, N Spain. Sedimentology, 2010, 36, 665-684.
[51] Bustillo M.A., Arribas M.E., Bustillo M., Dolomitization and silicification in low-energy lacustrine carbonates (Paleogene, Madrid Basin, Spain). Sedimentary Geology, 2002, 151, 107-126.
[52] Hargrave J.E., Hicks M.K., Scholz C.A., Lacustrine Carbonates from Lake Turkana, Kenya: A Depositional Model of Carbonates in an Extensional Basin. Journal of Sedimentary Research, 2014, 84, 224-237.
[53] Huang Q.Y., Zhang S.N., Zhang S.Y., Liu D., Ye N., Textural control on development of dolomite reservoir: a study from the cambrian-ordovician dolomite, central tarim basin, NW china. Natural Gas Geoscience, 2014, 25, 341-350 (in Chinese with English abstract).
[54] Glover J.E., Significance of stylolites in dolomitic limestones. Nature, 1968, 217, 835-836.
[55] Hugman R.H.H., Friedman M., Effects of texture and composition on mechanical behavior of experimentally deformed carbonate rocks. AAPG Bulletin, 1979, 63, 1478-1489.
[56] Jin Z.J., Zhu D.Y., Hu W.X., Zhang X., Zhang J., Mesogenetic dissolution of the middle ordovician limestone in the tahe oilfield of tarim basin, NW China. Marine and Petroleum Geology, 2009, 26, 753-763.
[57] Mazzullo S.J., Harris P.M., Mesogenetic dissolution: its role in porosity development in carbonate reservoirs. AAPG Bulletin, 1992, 76, 607-620.

[58] Zhu D.Y., Zhang D.W., Zhang R.Q., Role of oil charge in preservation of deep dolomite reservoir space. Acta Geologica Sinica, 2015, 89, 794-804 (in Chinese with English abstract).